PHYSICAL REVIEW B **79**, 045133 (2009)

Dual fermion approach to the two-dimensional Hubbard model: Antiferromagnetic fluctuations and Fermi arcs

A. N. Rubtsov,[1] M. I. Katsnelson,[2] A. I. Lichtenstein,[3] and A. Georges[4]
[1]*Department of Physics, Moscow State University, 119992 Moscow, Russia*
[2]*Institute for Molecules and Materials, Radboud University, 6525AJ Nijmegen, The Netherlands*
[3]*Institute of Theoretical Physics, University of Hamburg, 20355 Hamburg, Germany*
[4]*Centre de Physique Theorique, CNRS, Ecole Polytechnique, 91128 Palaiseau Cedex, France*
(Received 20 October 2008; published 30 January 2009)

We present an efficient diagrammatic method to describe nonlocal correlation effects in lattice fermion Hubbard-type models, which is based on a change of variables in the Grassmann path integrals. The new fermions are dual to the original ones and correspond to weakly interacting quasiparticles in the case of strong local correlations in the Hubbard model. The method starts with dynamical mean-field theory as a zeroth-order approximation and includes nonlocal effects in a perturbative way. In contrast to cluster approaches, this method utilizes an exact transition to a dual set of variables. It therefore becomes possible to treat vertices of an effective *single-impurity* problem as small parameters. This provides a very efficient interpolation between bandlike weak-coupling and atomic limits. The method is illustrated on the two-dimensional Hubbard model. The antiferromagnetic pseudogap, Fermi-arc formations, and non-Fermi-liquid effects due to the Van Hove singularity are correctly reproduced by the lowest-order diagrams. Extremum properties of the dual fermion approach are discussed in terms of the Feynman variational principle.

DOI: 10.1103/PhysRevB.79.045133 PACS number(s): 71.10.Fd, 71.27.+a, 71.30.+h

I. INTRODUCTION

One of the most successful theories of strongly correlated fermions on a lattice is dynamical mean-field theory (DMFT).[1] Physically, this approach treats the local spin and orbital fluctuations of the correlated electrons in a correct self-consistent way, while the spatial intersite correlations on the lattice are neglected. The nonperturbative DMFT approach is successful because a number of the most important correlation effects are indeed related to local fluctuations. For example, DMFT describes correctly phenomena such as the local moment formation in itinerant magnets,[2] some aspects of Kondo physics,[3] and the Mott insulator-to-metal transition on a lattice with a large connectivity in high-dimensional materials.[1]

On the other hand, there is increasing evidence that the nonlocality of spatial correlations plays an important role, particularly for the Luttinger-liquid physics of low-dimensional correlated systems,[4] *d*-wave pairing in quasi-two-dimensional (2D) cuprates,[5,6] and non-Fermi-liquid behavior due to Van Hove singularities in two-dimensional systems.[7–9] Moreover, angle-resolved photoemission spectra of three-dimensional ferromagnetic iron shows appreciable *k*-dependent self-energy effects.[10]

The most obvious generalizations of DMFT that take into account the short-range nonlocal fluctuations are the so-called cluster-DMFT (CDMFT) approximations, in real or *k* space.[11,12] In these methods, correlations are assumed to be localized within a cluster including several lattice sites. Cluster methods do catch the basic physics of *d*-wave pairing and antiferromagnetism in high-T_c superconductors[13,14] and the effects of intersite Coulomb interaction in transition-metal oxides.[15] At the same time, the complicated *k* dependence of the self-energy close to the Fermi surface, giving rise to Luttinger-liquid formation, is related to long-range fluctuations and therefore cannot be described within cluster approaches. For the same reason, cluster methods hardly can handle the effects due to Van Hove singularities or nesting.[7,9] Another drawback of the cluster methods is that the specific choice of the cluster and corresponding self-consistency condition is not unique. Different self-consistency conditions [e.g., dynamical cluster approximation (DCA) (Ref. 12) and free-cluster CDMFT (Ref. 11)] or periodization schemes (e.g., self-energy and cumulant periodization[14]) can result in physically different solutions. For example, the critical temperature of the *d*-wave superconducting transition of the doped Hubbard model is different in DCA calculations[12] and for then 2×2 free cluster.[14]

The present paper is devoted to an alternative extension of DMFT, which operates with a *single-site* impurity problem and treats spatial nonlocality in a diagrammatic way. Let us first recall the key DMFT equations. Formally, the assumption of local correlations means that the environment of a correlated atom can be replaced with a Gaussian effective medium. Consequently, the lattice problem reduces to the impurity problem. The latter is described by the effective impurity action

$$S_{\mathrm{imp}} = S_{\mathrm{at}} + \sum_{\omega,\sigma} \Delta_{\omega} c^{*}_{\omega,\sigma} c_{\omega,\sigma}, \tag{1}$$

where S_{at} is an action of the isolated or bare atom, and the second term is the hybridization due to the rest of the lattice. An important property of the DMFT approach is that this hybridization function has nontrivial frequency dependence, so that the approximation catches the physics of local fluctuations of spin, charge, and orbital degrees of freedom. For example, it is vital for the description of Kondo physics.[3]

It is obvious that the impurity problem is much simpler than the original lattice one. Nowadays, a number of numeri-

cally efficient impurity solvers are available. In particular, these solvers allow one to calculate the Green's function of the impurity problem $g_{\omega,\sigma}$ on the Matsubara frequencies' axis. This is the only property of the impurity problem entering in the DMFT self-consistent equations. The DMFT approximation for the Green's function of the initial lattice problem corresponds to the following expression:

$$G^{\mathrm{DMFT}}_{\omega k\sigma} = \frac{1}{g^{-1}_{\omega,\sigma} + \Delta_{\omega,\sigma} - \epsilon_k}. \tag{2}$$

One can see from this equation that the self-energy is local in DMFT since the momentum dependence of ϵ_k is not renormalized. The hybridization function Δ satisfies the self-consistency condition of DMFT,

$$G^{\mathrm{DMFT}}_{r=0,\omega,\sigma} = g_{\omega,\sigma}, \tag{3}$$

where $G_{r=0}=N^{-1}\Sigma_k G_k$ is the local part of Green's function (2) of the lattice with N sites.

In order to understand the main idea of the present work, let us first describe in a simple way DMFT condition (3). If we consider the case of a truly Gaussian system, then the DMFT approach becomes exact. For this case, Eq. (3) is trivial. Indeed, to obtain the impurity problem for the site j, one integrates out truly Gaussian degrees of freedom for other sites. This exact procedure does not change the properties of the electron motion at the site j, so the local part of the Green's function before integration must equal the Green's function after the integration, $G_{R=0}=g$. Turning back to the general case of a non-Gaussian ensemble, we note that among different properties of the impurity model, the DMFT scheme uses only the local Green's function $g_{\omega\sigma}$. Once $g_{\omega\sigma}$ is known, the approximation does not differ between Gaussian and non-Gaussian cases. Therefore, if a certain equation for $g_{\omega\sigma}$ is established for the Gaussian limit, it must also remain valid for the general case.

As it follows from the previous discussion, the DMFT equations are essentially the formulas for the Gaussian limit, renormalized in terms of the Green's function of the impurity problem. It turns out that the resulting theory works well, not only in the case of weakly interacting systems, but also in the atomic limit case, which is very different from a Gaussian system. A good interpolation between the two different limits is a key advantage of the DMFT approach.

Starting with the above interpretation of DMFT, it is natural to discuss a possible extension of this theory. Such an extension should be based on the perturbation series near the Gaussian limit, renormalized in terms of the impurity problem. The lowest-order term of such a theory should restore the DMFT result, whereas higher-order corrections would describe spatial nonlocality. A properly constructed theory of this kind would describe both short- and long-range fluctuations and will not suffer from the periodization problems of cluster DMFT.

Unfortunately, the straightforward construction of such an extension meets serious difficulties. The problem is that the extension is not unique. Beyond DMFT, there are many ways to choose the renormalization procedure, to define the hybridization function for the impurity problem and other quantities. One can formulate the major requirements for the desirable nonlocal correlated theory. They include the following:

(a) At least in the Gaussian and atomic limits, the theory should become a regular series around DMFT, with an explicit small parameter.

(b) The basic conservation laws should be fulfilled in the theory.

(c) The choice of hybridization function should be optimal, in a certain sense.

(d) There should be good practical convergence of the series: the leading corrections should capture most of the nonlocal physics.

(e) Last but not least, the equations of the theory must be easy enough for practical calculations.

There have been several previous attempts to construct a proper theory of this kind.[16–18] These approaches require a solution of ladderlike integral equations for the complete vertex Γ and the subsequent use of the Bethe-Salpeter equation to obtain the Green's functions. The first step exploits the vertex part of the effective impurity problem, whereas the second step uses just the bare interaction parameter U. We do not know of detailed tests of these approaches,[16–18] but we suspect that the presence of bare U in the theory makes it suitable for the metallic phases only. We also note that ladderlike integral equations are hard for practical calculations.

In this paper, we describe in detail a formalism fulfilling all the criteria from the above list. A preliminary version of this method was published in Ref. 19. The method is based on the transition to the new set of variables, called the dual ensemble. The procedure utilizes a Hubbard-Stratonovich transformation for the Gaussian part of the action. Several years ago, this trick was first proposed for classical fluctuation fields.[20] For a strong-coupling expansion of the Hubbard model around the atomic limit without hybridization function, the equivalent Hubbard-Stratonovich transformation has been proposed in different papers.[21,22] A similar procedure for fermions with general nonlocal interactions has been discussed recently.[23] Also we would like to mention a much earlier work[24] for classical fields. Although it used a different formalism,[24] the resulting diagram series resembles ours.

The paper is organized as follows. Section II is devoted to the general theoretical framework. Section III describes the application of the nonlocal theory to the problem of the antiferromagnetic pseudogap and the formation of Fermi arcs in the two-dimensional Hubbard model for high-temperature superconducting cuprates. In Appendix A we discuss how the many-particle excitations for the initial and dual systems are related. In Appendix B the functional-minimization derivation of the self-consistent DMFT condition is discussed.

II. DUAL FERMION FORMALISM: BEYOND DMFT

A. Definitions

We start from the two-dimensional Hubbard model with the corresponding imaginary-time action

$$S[c,c^*] = \sum_{\omega k\sigma} (\epsilon_k - \mu - i\omega) c^*_{\omega k\sigma} c_{\omega k\sigma} + U \sum_i \int_0^\beta n_{i\uparrow\tau} n_{i\downarrow\tau} d\tau. \tag{4}$$

Here β and μ are the inverse temperature and chemical potential, respectively, $\omega=(2j+1)\pi/\beta$, with $j=0,\pm 1,\ldots$, are the Matsubara frequencies, τ is imaginary time, and $\sigma=\uparrow,\downarrow$ is the spin projection. The bare dispersion law is $\epsilon_k=-2t(\cos k_x+\cos k_y)$. c^*,c are Grassmann variables, and $n_{i\sigma\tau}=c^*_{i\sigma\tau}c_{i\sigma\tau}$, where the indices i and k label sites and quasimomenta.

In the spirit of the DMFT, we introduce a single-site reference system (an effective impurity model) with the action

$$S_{\rm imp} = \sum_{\omega,\sigma} (\Delta_\omega - \mu - i\omega) c^*_{\omega,\sigma} c_{\omega,\sigma} + U \int_0^\beta n_{\uparrow\tau} n_{\downarrow\tau} d\tau, \tag{5}$$

where Δ_ω is a yet undefined hybridization function describing the interaction of the effective impurity with a bath. We assume that all properties of the impurity problem such as single-particle Green's function g_w and higher momenta can be calculated. In particular, we will use the fourth-order vertex $\gamma^{(4)}_{1234}=g^{-1}_{11'}g^{-1}_{22'}(\chi_{1'2'3'4'}-g_{1'4'}g_{2'3'}+g_{1'3'}g_{2'4'})g^{-1}_{3'3}g^{-1}_{4'4}$. (Here, χ is a two-particle Green's function of the impurity problem, and indices stand for a combination of σ and ω; for example, $g_{11'}$ means $g_{\sigma_1,\omega_1,\sigma_{1'},\omega_{1'}}$.) Our goal is to express the Green's function $G_{\omega k}$ and other properties of the lattice problem of Eq. (4) via the quantities for the impurity problem.

B. Dual variables: Exact formulas

Since Δ is independent of k, lattice action (4) can be represented in the following form:

$$S[c,c^*] = \sum_i S_{\rm imp}[c_i,c_i^*] - \sum_{\omega k\sigma} (\Delta_\omega - \epsilon_k) c^*_{\omega k\sigma} c_{\omega k\sigma}. \tag{6}$$

We utilize a dual transformation to a set of new Grassmann variables f,f^*. The identity

$$e^{A^2 c^*_{\omega k\sigma} c_{\omega k\sigma}} = \left(\frac{A}{\alpha}\right)^2 \int e^{-\alpha(c^*_{\omega k\sigma} f_{\omega k\sigma} + f^*_{\omega k\sigma} c_{\omega k\sigma}) - \alpha^2 A^{-2} f^*_{\omega k\sigma} f_{\omega k\sigma}} \times df^*_{\omega k\sigma} df_{\omega k\sigma} \tag{7}$$

is valid for arbitrary complex numbers A and α. We chose $A^2=(\Delta_\omega-\epsilon_k)$ for each set of indices ω,k,σ. The quantity α remains yet unspecified, but we require it to be dispersionless; $\alpha=\alpha_{\omega,\sigma}$.

With this identity, the partition function of the lattice problem $Z=\int e^{-S[c,c^*]}\mathcal{D}c^*\mathcal{D}c$ can be presented in the form $Z=\int\int e^{-S[c,c^*,f,f^*]}\mathcal{D}f^*\mathcal{D}f\mathcal{D}c^*\mathcal{D}c$, where

$$S[c,c^*,f,f^*] = -\sum_{\omega k} \ln[\alpha^2_{\omega\sigma}(\Delta_\omega - \epsilon_k)] + \sum_i S_{\rm imp}[c_i,c_i^*] + \sum_{\omega k\sigma} [\alpha_{\omega\sigma}(f^*_{\omega k\sigma} c_{\omega k\sigma} + c^*_{\omega k\sigma} f_{\omega k\sigma}) + \alpha^2_{\omega\sigma}(\Delta_\omega - \epsilon_k)^{-1} f^*_{\omega k\sigma} f_{\omega k\sigma}]. \tag{8}$$

As a next step, we establish an exact relation between the Green's function of the initial system $G_{\tau-\tau',i-i'}=-\langle Tc_{\pi i}c^*_{\tau' i'}\rangle$ and that of the dual system $G^{\rm dual}_{\tau-\tau',i-i'}=-\langle Tf_{\pi i}f^*_{\tau' i'}\rangle$. To this aim, we can replace $\epsilon_k\to\epsilon_k+\delta\epsilon_{\omega k}$ with a differentiation of the partition function with respect to $\delta\epsilon_{\omega k}$. Since we have two expressions for actions (4) and (8), one obtains

$$G_{\omega,k} = (\Delta_\omega - \epsilon_k)^{-1} \alpha_{\omega\sigma} G^{\rm dual}_{\omega,k} \alpha_{\omega\sigma} (\Delta_\omega - \epsilon_k)^{-1} + (\Delta_\omega - \epsilon_k)^{-1}. \tag{9}$$

Similar relations hold also for higher-order momenta, as Appendix A describes.

The crucial point is that the integration over the initial variables c_i^*,c_i can be performed separately for each lattice site since α is local and $\Sigma_k(f^*_k c_k + c^*_k f_k)=\Sigma_i(f^*_i c_i + c^*_i f_i)$. For a given site i, one should integrate out c_i^*,c_i from the action that equals

$$S_{\rm site}[c_i,c_i^*,f_i,f_i^*] = S_{\rm imp}[c_i,c_i^*] + \sum_\omega \alpha_{\omega\sigma}(f^*_\omega c_\omega + c^*_\omega f_\omega). \tag{10}$$

We finally obtain an action S depending on the new variables f,f^* only:

$$S[f,f^*] = -\sum_{\omega k} \ln[\alpha^{-2}_{\omega\sigma}(\Delta_\omega - \epsilon_k)] - \sum_i \ln z_i^{\rm imp} + \sum_{\omega k\sigma} \alpha_{\omega\sigma}[(\Delta_\omega - \epsilon_k)^{-1} + g_\omega]\alpha_{\omega\sigma} f^*_{\omega k\sigma} f_{\omega k\sigma} + \sum_i V_i, \tag{11}$$

where $z_i^{\rm imp}=\int e^{-S_{\rm imp}[c_i^*,c_i]}\mathcal{D}c_i^*\mathcal{D}c_i$, and the dual potential $V_i \equiv V[f_i^*,f_i]$ is defined from the expression

$$\int e^{-S_{\rm site}[c_i^*,c_i,f_i^*,f_i]}\mathcal{D}c_i^*\mathcal{D}c_i = z_i^{\rm imp} \exp\left(\sum_{\omega\sigma} \alpha^2_{\omega\sigma} g_\omega f^*_{\omega i\sigma} f_{\omega i\sigma} - V[f_i,f_i^*]\right). \tag{12}$$

The Taylor series for $V[f_i,f_i^*]$ can be obtained from the expansion of this definition in powers of f_i,f_i^*. One can see that Eq. (12) defines V in such a way that this series starts from the quartic term, $\propto f^*f^*ff$. Later on we take, for convenience,

$$\alpha_{\omega\sigma} = g_\omega^{-1}, \tag{13}$$

as it gives a particularly simple form of V. In this case the leading term in V is $-\frac{1}{4}\gamma^{(4)}_{1234}f^*_1 f^*_2 f_3 f_4$. Further Taylor-series terms yield similar combinations including $\gamma^{(n)}$ of higher orders.

Thus we see that in the dual action, the interaction terms remain localized in space, but they are nonlocal in imaginary time since, for example, $\gamma^{(4)}$ depends on the three independent Matsubara frequencies. Except for this point, action (11) formally resembles Eq. (4).

There is a point which is worthwhile to discuss here: one can formally apply transformation (7) with some new hybridization function to dual system (11), and thus obtain a sequence of changes to new variables. It is useless, however, since mathematically, these transformations form a group. It is easy to show that any sequence of transformation (7) corresponds to a single change of variables with a certain Δ. Moreover, there is an *inverse* change of variables that allows

one to obtain $S[c,c^*]$ back from the $S[f,f^*]$. It is given just by Eq. (7) with A replaced with αA^{-1}.

C. Gaussian approximation for dual ensemble and the relation to DMFT

Since the transformation from initial system (4) to action (11) contains no approximations, it is equally hard to describe exactly the properties of c^*,c fermions as thereof dual fermions. The main idea of switching to the new variables is that for a properly chosen Δ, correlation properties of the f^*,f system are simpler than for the c^*,c original model. In other words, the magnitude of the nonlinear part in the dual action can be effectively decreased by the proper choice of Δ. To illustrate this statement, let us just neglect V in Eq. (11). We denote the Green's function for such Gaussian approximation for the dual potential with calligraphic letters. Expression (11) corresponds to

$$\mathcal{G}^{\text{dual}}_{\omega,k} = -g_\omega[(\Delta_\omega - \epsilon_k)^{-1} + g_\omega]^{-1} g_\omega. \tag{14}$$

Being combined with identity (9), this gives the formula

$$\mathcal{G}_{\omega,k} = (g_\omega^{-1} + \Delta_\omega - \epsilon_k)^{-1}. \tag{15}$$

One can recognize that this is exactly a DMFT expression for the Green's function. Therefore we conclude that for a properly chosen Δ a Gaussian approximation for the dual potential already yields a reasonable result, as DMFT does. It is important to point out that DMFT works well for the whole range of the parameters. In contrast, the Gaussian approximation for the atomic limit of initial model (4) makes no sense. In that aspect, the dual potential V is indeed smaller than U.

An argumentation can be presented to justify that the DMFT value of Δ is a proper choice for Gaussian approximation (15). One of the reasons is described in Appendix B. It turns out that the Feynman minimization criterion for the Gaussian trial action, being formulated for the dual ensemble, gives exactly the DMFT hybridization function. Another argument is presented in Sec. II D.

Once the dual potential is taken into account, it yields a correction to the DMFT result. It is useful to introduce the dual self-energy

$$\Sigma_{\text{dual}} \equiv \mathcal{G}^{-1}_{\text{dual}} - G^{-1}_{\text{dual}}, \tag{16}$$

and the correction to the DMFT self-energy

$$\Sigma' \equiv \mathcal{G}^{-1} - G^{-1}. \tag{17}$$

With these quantities, we can re-express exact relation (9) in a particularly simple form,

$$\Sigma'^{-1}_{\omega,k} = g_\omega + (\Sigma^{\text{dual}}_{\omega,k})^{-1}. \tag{18}$$

We note that this expression relates quite different quantities: Σ_{dual} and Σ' characterize the corresponding lattice problems and carry, in general, both momentum and frequency dependences, whereas g comes from the impurity model and is local in space.

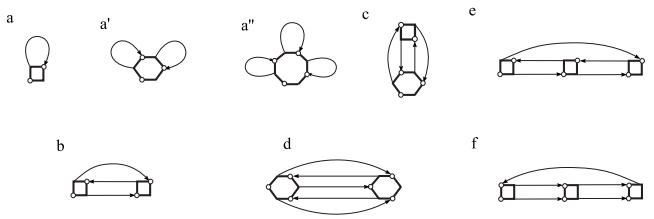

FIG. 1. Various diagrams for Σ^{dual}. Diagrams (a), (a′), and (a″) are vanished by condition (19).

D. Diagram series: General properties and the choice of hybridization function

The main idea of our method is to consider a diagrammatic expansion with respect to the dual potential V. We will later demonstrate that in point of fact low-order diagrams of such a series bring important information about nonlocal correlations. The basic reasoning for this is presented in Sec. II C: since the value of V is in certain sense small, the first few terms of the perturbation series with respect to V can make sense. More detailed discussions about the small parameters of the theory are presented in Secs. II E and II F; let us first present the general properties of the diagrams under consideration.

The rules of diagram construction are quite similar to the usual Matsubara diagram technique. The only difference from the standard perturbation scheme is that the interaction operator V is not purely of the fourth-order form f^*f^*ff, and therefore vertices in the diagrams are not necessarily four legged, but may formally have any even number of legs. For choice (13), these vertices are essentially $\gamma^{(n)}$. They are connected with the lines being the dual Green's functions. Some of the diagrams contributing to the dual self-energy are presented in Fig. 1.

We use the skeleton diagrams with renormalized Green's functions, so that the lines are complete G_{dual} and not $\mathcal{G}_{\text{dual}}$. The reason to use the skeleton-diagram expansion for the dual self-energy is that it makes it possible to obtain conserving theories, similar to conventional diagram technique.[25] The Baym criterion of a conservative theory is the existence of a functional of the Green's function $\Phi[G]$ such that $\frac{\delta\Phi}{\delta G} = \Sigma$. Once this functional is described by certain skeleton diagrams, taking the derivative means just cutting the lines in that diagram. For example, diagrams (a) and (b) for the self-energy come from diagrams (a_Φ) and (b_Φ), shown in Fig. 2 (of course, care should be taken of the numerical factors). Second-order differentiation with respect to G gives the two-particle quantities. Such a procedure automatically produces a theory fulfilling the conservation laws for energy, momentum, particle numbers, etc.

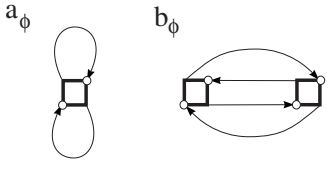

FIG. 2. Two simple diagrams for Baym functional $\Phi_{\text{dual}}[G_{\text{dual}}]$. Functional differentiation of these diagrams with respect to G_{dual} produces diagrams (a) and (b) for self-energy.

In our consideration, the usage of skeleton diagrams describes a corresponding Baym functional $\Phi_{\text{dual}}[G_{\text{dual}}]$ with the functional derivative being Σ_{dual}. Therefore, it produces a conservative approximation for the dual ensemble. Then it turns out that exact transformations (9) and (A5) give a conserving description of the initial system. Simply, the conservation laws imply certain selection rules for G and Γ, and Eqs. (9) and (A5) clearly preserve those selection rules during the transformation from dual to initial quantities. More precisely, the conserving character of an approximation in fact means that there exists some conserving dual action $\tilde{S}[f,f^*]$, exactly corresponding to this approximation. Since there is a one-to-one correspondence between $S[f,f^*]$ and $S[c,c^*]$ (see the end of Sec. II B), we conclude that the initial system described by a certain $\tilde{S}[c,c^*]$ is also conserving.

Until now, the hybridization function Δ has formally not been specified. Now, we establish a condition for Δ that corresponds to a particular condition for the diagrammatic series. Let us again consider the DMFT. Suppose that we want to obtain the DMFT result without DMFT loops, that is, using Δ_ω *not fulfilling* Eq. (B5). Formally, it is possible: one should just sum up all the diagrams containing a single vertex [diagrams (a), (a′), (a″), etc.]. Since these diagrams give exactly the DMFT self-energy, such a procedure would indeed recover the DMFT result for an arbitrary hybridization function. The special DMFT choice of Δ just allows one to eliminate such an infinite summation since Eq. (B6) eliminates all the diagrams containing a simple closed loop. It is reasonable to keep this property in higher approximations, that is, to require

$$G^{\text{dual}}_{\omega,r=0} = 0 \tag{19}$$

as a condition for Δ. Then, all the diagrams with simple closed loops drop out from the calculation. Note that these diagrams however should be taken into account while taking the functional derivatives. For example, the DMFT vertex part $\Gamma_{\text{dual}} = \gamma^{(4)}$ comes out from the differentiation of diagram (a). Finally, condition (19) obviously passes into Eq. (B6) at the DMFT limit. Therefore, until the corrections to DMFT are significant, one can approximate Δ_ω with the DMFT hybridization function.

The vanishing of the closed loops seriously reduces the number of the low-order dual diagrams. In most of the practical calculations presented below we consider a single diagram (b). It is clear that any reasonable expansion starts from this perturbation, and that this diagram already incorporates some nonlocal physics. The corresponding formula for the dual self-energy reads (spin and orbital indices are omitted)

$$\Sigma^{\text{dual}}_{\omega,r} = \frac{1}{2\beta^2} \sum_{\omega+\omega'=\omega_1+\omega_1} \gamma^{(4)}_{\omega\omega'\omega_1\omega_2} \gamma^{(4)}_{\omega_2\omega_1\omega'\omega} G^{\text{dual}}_{\omega_1,r} G^{\text{dual}}_{\omega_2,r} G^{\text{dual}}_{\omega',-r}. \tag{20}$$

E. Causal properties

Beyond conservation laws, the Green's function should be causal. The retarded Green's function $G^R(t)$, that is, an analytical continuation of G_τ to the real-time axis, should vanish for negative time:

$$G^R(t<0) = 0. \tag{21}$$

In the Fourier representation, condition (21) implies the analyticity of G_ω in the upper complex plane, as this follows directly from the definition of the Fourier transform. The inverse is also true. If the Fourier transform of a function is analytical in the upper plane, the function is causal. To prove this statement, it is enough to transform the integration contour of the inverse Fourier transform away from the real axis.

Frequently, the causality principle is associated with the positiveness of the imaginary part of the Green's function in the real-frequency domain. For dual Green's function, this can lead to certain misunderstanding. It is clear from condition (19) that the imaginary part of G^{dual} cannot be always positive. However, this issue is purely formal. Condition (21) itself does not imply that Im G_ω is positive. A trivial counterexample is the function $-G^R$. It fulfills Eq. (21) and has an always-negative imaginary part. We will argue the same for G^{dual}. It fulfills Eq. (21), although its imaginary part is not always positive.

Let us illustrate this statement at the zeroth order of the theory, single-site DMFT. It has been proven[1,11,12] that this theory is causal, so $\mathcal{G}$ and g fulfill Eq. (21). One can easily check, from expressions (14) and (15), that for the case of DMFT, a simple relationship holds; $\mathcal{G}^{\text{dual}} = \mathcal{G} - g$. It is immediately clear from this formula that since $\mathcal{G}$ and g are causal, $\mathcal{G}^{\text{dual}}$ also fulfills Eq. (21). Note again, condition (19) is fulfilled in DMFT, and $-\text{Im}\,\mathcal{G}^{\text{dual}}_\omega$ is therefore essentially nonpositive.

Let us now consider the dual fermion theory beyond DMFT. We will show that if the hybridization function Δ is casual, the resulting Green's function is also causal. First of all, the casuality of Δ is inherited from g and $\gamma^{(n)}$. Therefore, the dual system is characterized by the casual bare propagator $\mathcal{G}^{\text{dual}} = \mathcal{G} - g$ and casual interaction operator. Therefore, the theory with skeleton diagrams results in a causal G^{dual}.[26] Finally, it should just be proven that the casuality G^{dual} means the casuality of G. The latter statement follows from exact relation (9). Indeed, since $\alpha \equiv g_\omega$ does not have zeros in the upper plane, g^{-1}_ω is analytical. The same is true for the quantity $(\Delta - \epsilon)^{-1}$. Therefore, the entire right-hand side of Eq. (9) is analytical in the upper plane. This implies the causality of G.

In the calculation procedure described below, we always start from a causal Δ and change it iteratively to deliver condition (19). We will argue that such an iteration procedure preserves the causality of Δ. Therefore, the entire theory is causal.

Finally, let us recall the issue of the positiveness of $-\text{Im}\,G$ in the complex upper plane. Actually, this is related with the positivity of the residuals, as it follows from the Lehmann representation $G = \Sigma(Z_{mn}/\omega - \omega_{mn} + i\delta_{mn})$. Here, the causality follows from the positivity of δ, whereas the requirement $Z > 0$ ensures that $-\text{Im}\,G > 0$. For our theory, we were not able to prove the positivity of the residuals formally. However, we do not consider this as a serious drawback since our practical calculations always produce undoubtedly positive residuals.

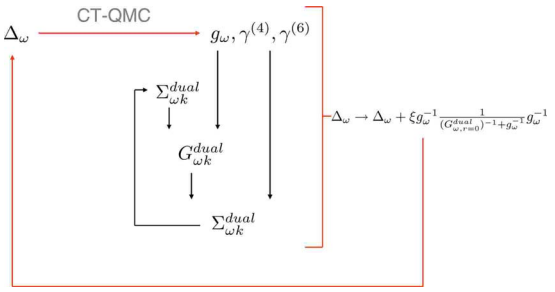

FIG. 3. (Color online) The scheme of calculation. The calculation includes "big" and "small" loops, marked with red and black lines, respectively. The small loop is for determining the renormalized dual Green's function G^{dual} in a self-consistent way, for given Δ, g, and $\gamma^{(n)}$. The big loop is for determining Δ. Only the big loop requires a solution of the impurity problem.

F. Small parameter in the extreme cases

An important property of the DMFT approach is that it becomes exact for the two opposite cases of a noninteracting Gaussian system and of an extreme strong-coupling limit corresponding to the atomic limit.[1] The dual fermion formalism inherits this property; moreover the corresponding smallness appears in the diagrams in a simple form. Let us first consider the strong-coupling limit $\epsilon_k \to 0$. It is useful to estimate the DMFT dual Green's function $\mathcal{G}$, defined by formula (14) and condition (19). For a pure atomic limit $\epsilon_k = 0$, the Green's function is local, $\mathcal{G}_{r\neq 0} = 0$. However, the local part of the Green's function also vanishes due to condition (19). Formally, $\mathcal{G} \to 0$ as $\Delta \to 0$. The smallness of ϵ and Δ allows the approximate estimation of the dual Green's function near the atomic limit. It gives $\mathcal{G}_{\omega k} \approx g_\omega \epsilon_k g_\omega$. Since the DMFT is almost exact near the atomic limit, the same estimation is valid for G^{dual}. Consequently, *near the atomic limit the lines in the dual diagrams carry a small factor* ϵ_k.

On the other hand, for the opposite weak-coupling limit $U \to 0$, the vertex parts of the impurity problem can be estimated as $\gamma^{(4)} \propto U$, $\gamma^{(6)} \propto U^2$, etc. Therefore, *for the weak-coupling limit the vertices in the dual diagrams are manifestly small.*

The presence of a small parameter in these two limits does not guarantee a good interpolation between them. It should however be mentioned that the scheme performs well if the corrections to DMFT are small: for this case we deal in fact with a perturbation series around DMFT. The validity of the method for more general situations should be checked in practical calculation. This practical validity depends on the particular choice of diagrammatic approximation for Σ_{dual}. In this context, it is worthy to discuss the choice of hybridization function Δ.

G. Calculation procedure

In practical calculations the solution was obtained iteratively, similarly to the DMFT loop. The iterative scheme is presented in Fig. 3. It includes the big (outer) and small (inner) loops. The small loop is devoted to obtaining the dual Green's function and self-energy, given the solution of the impurity model with certain Δ. It starts from some guess for Σ_{dual}, for instance, $\Sigma^{(0)}_{\mathrm{dual}} = 0$. The dual Green's function $(\mathcal{G}^{-1}_{\mathrm{dual}} - \Sigma_{\mathrm{dual}})^{-1}$ is substituted in formula (20) to produce a new estimation for Σ_{dual}. The procedure is repeated until converging results are reached.

The big loop is very similar to the DMFT iterative procedure. We start with some initial guess for Δ and solve an impurity model. We use the weak-coupling continuous time quantum Monte Carlo (CT-QMC) solver,[27] which produces both the Green's function g and the four-point vertex $\gamma^{(4)}$ in the frequency domain. Then we perform the inner loop to obtain G_{dual} (this step is not necessary in DMFT since it uses the bare dual Green's function $\mathcal{G}_{\mathrm{dual}}$). Finally, we take a new guess for the hybridization function

$$\Delta_\omega \to \Delta_\omega + \xi g_\omega^{-1} \frac{1}{(G^{\mathrm{dual}}_{\omega,r=0})^{-1} + g_\omega^{-1}} g_\omega^{-1} \tag{22}$$

and repeat the self-consistent procedure. A value of the parameter $\xi \leq 1$ was chosen to ensure better convergence. The last formula is organized in such a way that: (i) its fixed point clearly satisfies condition (19) and (ii) for $\Sigma_{\mathrm{dual}} = 0$ it passes into the DMFT update formula $\Delta_\omega \to \Delta_\omega + \xi(\mathcal{G}^{-1}_{\omega,r=0} - g_\omega)$. Of course, only requirement (i) is actually necessary, so that formula (22) is not unique. In particular, it is useful to consider an update

$$\Delta_\omega \to \Delta_\omega + \xi g_\omega^{-1} G^{\mathrm{dual}}_{\omega,r=0} g_\omega^{-1}. \tag{23}$$

One can easily see that update (23) conserves causal properties of Δ, so that the convergence of iteration process (23) proves the causality of the result. Such a convergence indeed takes place for the calculations presented below. Note also that near the fixed point $G^{\mathrm{dual}}_{\omega,r=0} = 0$, formula (22) passes into Eq. (23), so that there is no much practical difference between these two formulas.

III. APPLICATION TO THE HUBBARD MODEL

In Secs. III A–III C, we present the results of our calculations for the 2D Hubbard model. We start with the half-filled case with next-nearest-neighbor hopping $t' = 0$ lattice. We compare our data with direct QMC simulations on a finite Hubbard lattice, which are relatively simple due to the absence of the sign problem for the half-filled Hubbard model.

Properties of the half-filled Hubbard model are well known and are mostly related to the antiferromagnetic phenomenon and Mott metal-insulator transition. Local magnetic moments on atoms are formed and tend to order into an antiferromagnetic lattice due to the effective superexchange coupling. At zero temperature, the antiferromagnetism arises already at $U = 0^+$ because of the perfect nesting. At finite temperature, the true antiferromagnetism is destroyed by the long-range fluctuations. However, short-range antiferromagnetic correlations are still present. Short-range antiferromagnetic ordering manifests itself as the strong pseudogap in the local electron spectral function.

We consider the system with $t = 0.25$ at inverse temperature $\beta = 20$, with different values of U. Since the temperature is relatively high, it is enough to use the reference data ob-

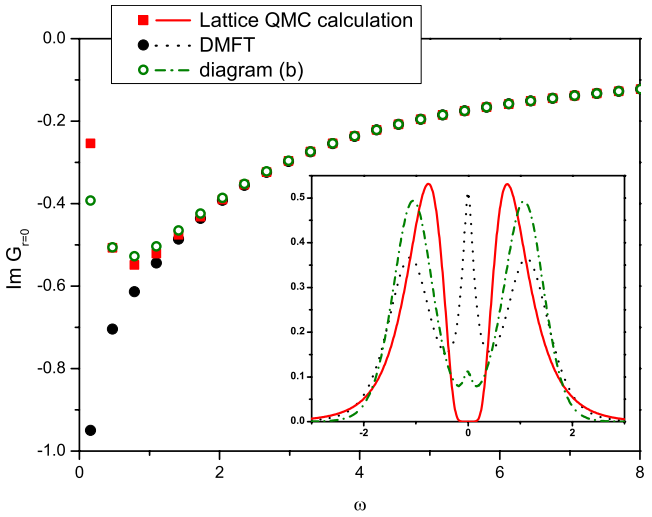

FIG. 4. (Color online) Local Green's function at Matsubara frequencies and density of states for undoped Hubbard model at $t=0.25, U=2.0, \beta=20$. The results of DMFT and the calculation with nonlocal diagram correction (b) are compared with the reference data obtained for 8×8 lattice QMC simulation.

tained just for the 8×8 lattice QMC simulation, with subsequent maximum-entropy continuation of the data to obtain local density of states (DOS). The results for paramagnetic calculation are presented in Figs. 4 and 6 (thin solid line). These results show that the narrow antiferromagnetic pseudogap is formed at approximately $U=1.0$. For larger U, the DOS contains also a wider Mott gap, having a half-width of about $U/2$. At $U=2.0$, the system shows essentially Mott-insulator DOS. The effect of antiferromagnetism in this case consists of the sharp shoulders of the Mott gap.

To understand better the physics of the half-filled Hubbard model, it is worthy to analyze the behavior of the electronic self-energy Σ. At small U, this is a small regular correction to the dispersion law ϵ_k. It follows from the weak-coupling analysis that $\mathrm{Im}\,\Sigma$ is strongly anisotropic in this regime, with peaks near $[0,\pm\pi],[\pm\pi,0]$ points. In contrast, for the truly antiferromagnetic gap, Σ_k would have a pole at the Fermi surface. The residue of this pole is the same at all points of the Fermi surface. For large enough U this pole is somehow shifted from the real-frequency axis due to long-range thermal fluctuations. But the qualitative picture remains the same: a sharp peak in $\mathrm{Im}\,\Sigma$, with almost constant magnitude along the Fermi surface.

It is well known that doping changes the physics of the Hubbard model substantially. First of all, a few-percent doping suppresses the antiferromagnetism. At higher doping values there is a trend to d-wave superconductivity. A superconducting phase has been obtained in various cluster-DMFT calculations[13,28] near the optimal doping of about 15%. This agrees well with the phase diagram of high-T_c cuprates.[6] The pseudogap formation in the doped Hubbard model was first analyzed by the cluster-DMFT method (more specifically, dynamical cluster approximation) in Ref. 29. For further applications of the DCA to the 2D Hubbard model, see Refs. 12 and 30–32. In the following consideration, we will not discuss the superconductivity itself, but we will address the so-called Fermi-arc phenomenon. Essentially, this is an anisotropic destruction of the Fermi surface in the pseudogap regime. Only the parts of Fermi surface near the nodal direction remain well defined at low temperature. In the antinodal direction, the spectral function at the Fermi level is vanishingly small.

A methodological difference between the doped and the undoped cases is that the sign problem makes direct lattice simulations away from half filling practically impossible.[33] Therefore, the reference point can only be the results of different approximate schemes or the experimental data.

A. Undoped case: Translationally invariant solution

First, we discuss the result of the dual fermion investigation without a spontaneous symmetry breaking, which means that the impurity problem is assumed to have no spin polarization. The data presented in this section have been partly discussed previously as a Brief Report.[19]

The translationally invariant DMFT predicts a Mott transition at rather high value $U>3.0$ (for a bandwidth $W=8t=2.0$). It is important to point out that the density of states at the Fermi energy is independent of U within the entire Fermi-liquid phase. This is a consequence of the locality of the self-energy in DMFT. Therefore, for $U\approx1.5-3.0$, the approximation predicts a three-peak DOS which consists of two Hubbard bands at $\pm U/2$ and a Kondo-type central peak providing the "pinned" value of DOS at Fermi level.

This behavior is inconsistent with the reference data described above. Actually, those data do not show a three-peak structure because of the antiferromagnetic pseudogap. Besides antiferromagnetism, the DMFT sufficiently overestimates the critical value of U for the Mott transition: according to the reference data, the system already shows DOS of the Mott-insulator nature at $U\approx2.0$ (see Fig. 4).

Let us take the leading dual diagram (b) into account. The corresponding data are presented in Figs. 4 and 5. Since the self-energy is not local anymore, there is no pinning at Fermi level, and the Kondo-type peak disappears. Furthermore, the self-energy momentum dependence agrees well with the qualitative picture described above. The upper panel of Fig. 5 presents contour plots for $\mathrm{Im}\,\Sigma_{\omega=0,k}$ at $U=1.0$ and $U=2.0$ (the data are obtained by a polynomial extrapolation from the Matsubara frequencies). The value of $\mathrm{Im}\,\Sigma_{\omega=0,k}$ grows dramatically as U changes from 1.0 to 2.0. At larger U, there is an expected sharp non-Fermi-liquid peak in $\mathrm{Im}\,\Sigma_{\omega=0,k}$ at Fermi level, without a remarkable anisotropy along Fermi surface. At smaller U, the peak is broadened, with maxima near Van Hove singularities. The renormalized dispersion law $\epsilon_k+\mathrm{Re}\,\Sigma_{\omega=0,k}$ is now also in qualitative agreement with numerical data, as shown in the lower panel of Fig. 5. In these graphs, $\epsilon_k+\mathrm{Re}\,\Sigma_{\omega=0,k}$ is compared with the reference data for a 10×10 lattice. There is a qualitative difference between the results for $U=1.0$ and $U=2.0$: for the latter case the corrections are quite large so that there is a dependence resembling ϵ_k^{-1}. The superiority of the result against DMFT should be stressed, as there is no k dependence of Σ in the DMFT approach.

Let us point out the drawbacks of the present results. First of all, there is still no perfect quantitative agreement with the

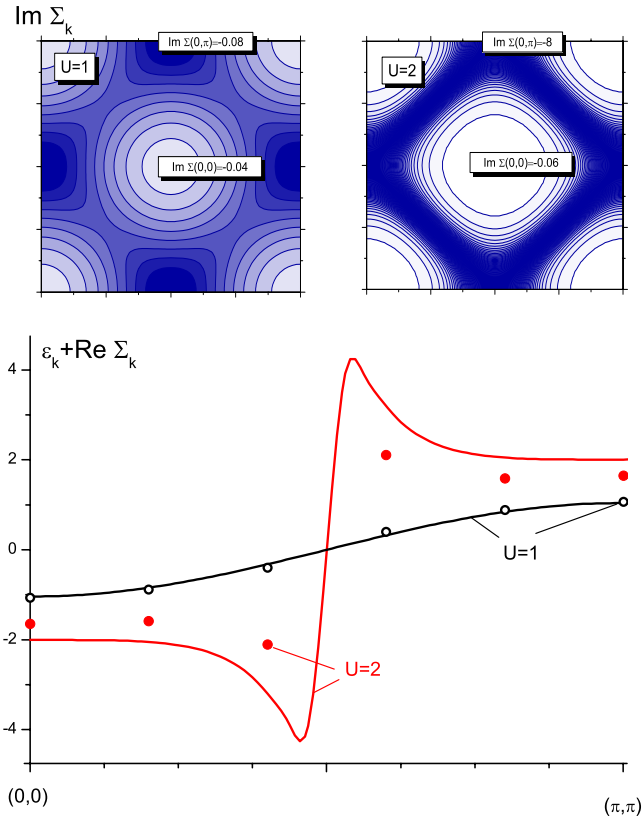

FIG. 5. (Color online) Momentum dependence for the self-energy function at Fermi energy, obtained with diagram (b) within the translationally invariant approximation for the undoped Hubbard model. Data are shown at $t=0.25, \beta=20$, for $U=1.0$ and $U=2.0$. Upper panel: contour plots for k dependence of the imaginary part of the self-energy. Lower panel: renormalized dispersion law $\epsilon_k+\mathrm{Re}\,\Sigma_{\omega=0,k}$, compared with the reference data obtained for 10×10 lattice. The figure has been published previously in a Brief Report (Ref. 19).

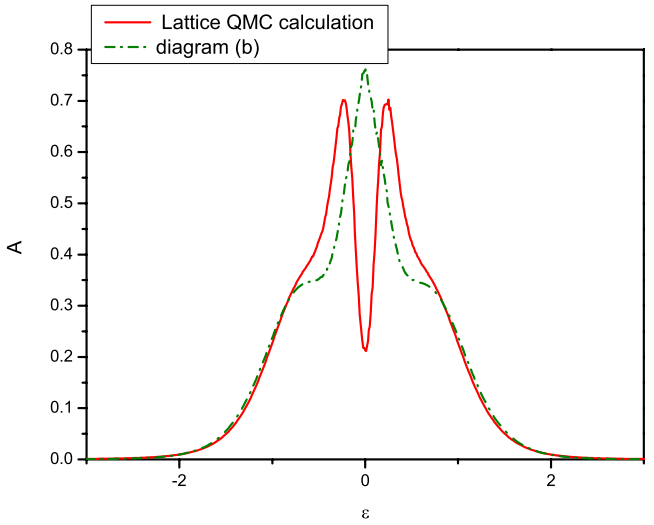

FIG. 6. (Color online) Density of states for undoped Hubbard model at $t=0.25, U=1.0, \beta=20$. The result of the translationally invariant calculation with diagram (b) is compared with the reference data for 8×8 lattice. An antiferromagnetic pseudogap is pronounced in the reference data and does not appear in the approximation.

reference data, although the DMFT result is improved remarkably. The source of this discrepancy becomes clear when the DOS for $U=1.0$ is plotted (Fig. 6). The pseudogap is much narrower in this case. It resembles the situation for $U\to+0$ at zero temperature; then an antiferromagnetic ordering appears due to long-range nesting phenomena. It is evident from Fig. 6 that the calculation with dual diagram (b) does not reproduce this pseudogap at all. Back to the results for $U=2.0$, the pseudogap in our calculation appears to be not as deep and not as steep as it should be (Fig. 4). We have tried to take higher diagrams into account and found out that it does not help much. We conclude that the dual fermion corrections, as they were considered above, improve the description of short-range Mott physics, but they do not take the long-range antiferromagnetic fluctuations into account.

To explain this failure, let us recall the Hubbard model with small U at zero temperature. As pointed above, our technique passes into weak-coupling diagram expansion for $U\to0$. But it is clear that the weak-coupling expansion is suitable for the metallic phase only and cannot reproduce the antiferromagnetism since this is a nonperturbative phenomenon.[34] Evidently, the dual fermion expansion inherits this property. The best possible achievement within this framework would be to obtain a phase transition, where the corresponding susceptibility diverges.[35]

There are two ways to take antiferromagnetism into account. First, one can switch from single-site to cluster DMFT. Thus the antiferromagnetic phase transition maintains the periodical symmetry of the superlattice made of clusters; there is no problem with nonanalyticity in this case. Indeed, various cluster-DMFT approaches[11,12] reproduce the antiferromagnetic gap. The dual fermion corrections can be used to improve the accuracy of those methods.[35,36]

The second option is to stay with the single-site starting point, but allow for the antiferromagnetic ordering on the lattice. In this case, the effective impurity problem is spin polarized. It is known that such an approach indeed works quite well already at the DMFT level.[37] It can be expected that the dual fermion technique can effectively provide the correction in this case. Section III B describes such a theory and the corresponding results.

B. Undoped case: Antiferromagnetic symmetry breaking

For clarity, let us present the explicit expressions for this case. The antiferromagnetism means that the primitive cell is doubled. The dual Green's function, as well as other single-electron quantities of the antiferromagnetic state, depends on the difference of the two coordinate arguments and single spin: $G^{\mathrm{dual}}_{\omega,j,s,j',s'}=G^{\mathrm{dual}}_{\omega,j-j',s}$ (note that s' is defined by s and $r=j-j'$). Given $G^{\mathrm{dual}}_{\omega,r,s}$, it is easy to obtain $\Sigma^{\mathrm{dual}}_{\omega,r,s}$ from formula (20). In this expression, the spin dependence of Σ comes from the spin polarizations of G^{dual} and, in principle, of the vertex $\gamma^{(4)}$. However, the numerical result for the latter quantity appears to be quite noisy. Therefore, we neglected the spin polarization of $\gamma^{(4)}$, performed an averaging over spin

orientation, and thus operated with the tensor of the "paramagnetic" symmetry. Such a tensor has the two independent components $\gamma' \equiv \gamma^{(4)}_{ssss}$ and $\gamma'' \equiv \gamma^{(4)}_{ss-s-s}$, so that expression (20) becomes

$$\sum^{\text{dual}}_{\omega,r,s} = \frac{1}{2\beta^2} \sum_{\omega+\omega'=\omega_1+\omega_1} \gamma'_{\omega\omega_1\omega'\omega_2} \gamma'_{\omega_2\omega'\omega_1\omega} G^{\text{dual}}_{\omega_1,r,s} G^{\text{dual}}_{\omega_2,r,s} G^{\text{dual}}_{\omega',-r,s} + \frac{1}{\beta^2} \sum_{\omega+\omega'=\omega_1+\omega_1} \gamma''_{\omega\omega_1\omega'\omega_2} \gamma''_{\omega_2\omega'\omega_1\omega} G^{\text{dual}}_{\omega_1,r} G^{\text{dual}}_{\omega_2,r,-s} G^{\text{dual}}_{\omega',-r,-s}. \quad (24)$$

We believe that this approximation is valid since the most important contribution to the symmetry break arises from the spin polarization of the single-electron quantities g, Δ, and Σ^{dual}, entering the expression for G^{dual}.

The next step is to write explicitly the definition $\Sigma_{\text{dual}} = \mathcal{G}^{-1}_{\text{dual}} - G^{-1}_{\text{dual}}$ in the momentum space. Here, the 2×2 matrices must be used, as the momentum is conserved up to $Q = (\pi, \pi)$. Let us denote $G^{\text{dual}(0)}_{\omega,j-j'} = \frac{1}{2}(G_{\omega,j-j',s} + G_{\omega,j-j',-s})$ and $G^{\text{dual}(\text{AF})}_{\omega,j-j'} = \frac{1}{2}(G_{\omega,j-j',s} - G_{\omega,j-j',-s})$. It is easy to check that the definition $\Sigma_{\text{dual}} = \mathcal{G}^{-1}_{\text{dual}} - G^{-1}_{\text{dual}}$ stays fulfilled with the matrix

$$\begin{pmatrix} G^{\text{dual}(0)}_k & G^{\text{dual}(\text{AF})}_k \\ G^{\text{dual}(\text{AF})}_k & G^{\text{dual}(0)}_{k+Q} \end{pmatrix}$$

used for G^{dual}, and similarly for $\Sigma_{\text{dual}}, \mathcal{G}_{\text{dual}}$. This gives a way to construct G^{dual} from a given Σ^{dual} and thus close the inner iteration loop. Self-consistency condition (19) remains unchanged, so that the big loop is essentially the same. Finally, exact relationship (9) can be written in the matrix form, giving thus a complete description of the antiferromagnetic state. Of course, the same treatment with $\Sigma^{\text{dual}} = 0$ corresponds to the antiferromagnetic DMFT.

Actually, once the antiferromagnetism is taken into account, the DMFT result itself is not too bad. The corresponding data are presented in Fig. 7, where we show how the Green's function at the lowest Matsubara frequency depends on U. At small U, the system is a normal Fermi liquid. There are small corrections due to the correlations. Of course, DMFT cannot reproduce the anisotropy of the self-energy, but the description of local Green's function is pretty good. For large U, the system exhibits a strong antiferromagnetism, which is destroyed only at long-range scale. In DMFT, the antiferromagnetic ordering appears in this range. The simplest way to take the long-range fluctuations into account within DMFT framework is to average over the two antiferromagnet sublattices. This eliminates the real part of the Green's function. A comparison of Im $G_{\pi/\beta,r=0}$ with lattice QMC simulations again shows good agreement. (The antiferromagnetic regime starts from $U \approx 0.85$, as the inset of Fig. 7 shows.) The largest deviations of the DMFT result from the reference data occur in the intermediate regime $U \approx 1$. Probably, in this regime the fluctuations are essentially nonlocal but still midrange. Therefore they cannot be described as a static long-range antiferromagnetic ordering.

The same Fig. 7 presents the result obtained with the first nonlocal dual diagram (b). In this calculation, we again allow for the antiferromagnetism. The symmetry breaks down at

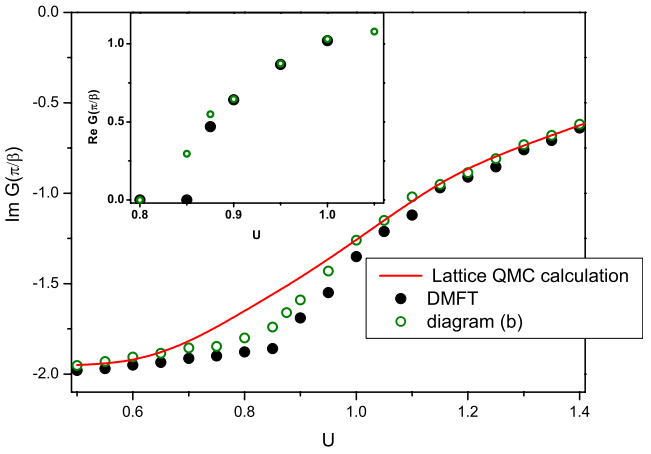

FIG. 7. (Color online) Results of DMFT calculation and the scheme with diagram (b), taking the antiferromagnetic ordering into account. The results for local part of the Green's function at lowest Matsubara frequency are compared with reference data for undoped Hubbard model at $t=0.25, \beta=20$. QMC calculations at 8×8 lattice are used for reference.

almost the same value of U, and the magnetization coincides with the DMFT result. There is however a remarkable correction to Im $G_{\pi/\beta,r=0}$. Near both limiting cases, the reference dependence is reproduced very well since diagram (b) yields a leading-order correction to the already good DMFT result. In the "critical" intermediate regime, the situation is not as good. However, the correction still behaves regularly and shows the correct trend. It is also important that while the DMFT data for Im $G_{\pi/\beta,r=0}$ show a clear kink at the transition point, the dual-diagram correction makes the curve much smoother. This is certainly more physical because the reference lattice QMC data contain no singularities since there is no true phase transition.

We did not found that any particular higher-order diagram improves the result for $G_{\pi/\beta,r=0}$ significantly. This indicates that a large number of higher-order diagrams contribute to the result. Actually, this is an expectable situation near the critical point. However, it was found that higher-order ladder corrections give a particularly important contribution to the spectral function of the system. Let us illustrate this statement, using the data for $U=1.0$. The Green's functions at Matsubara frequencies for this case are plotted in Fig. 8. Since the points with dual-diagram corrections are very close to the reference ones and can hardly be distinguished, we plot also the difference from the reference lattice QMC result in the inset of Fig. 8. Figure 9 shows the maximum-entropy guess for the corresponding DOS. Since the problem of analytical continuation of the Green's function to the real-frequency axis is known to be ill posed, we took special measures while calculating the density of states. The Green's functions are computed with high accuracy, and the maximum-entropy analytical continuation is performed with the same *a priori* parameters for all curves. This ensures that the graphs for the spectral function can be compared with each other. The spectral function clearly illustrates the physical origin of the discrepancy between the DMFT and reference data. Indeed, since DMFT replaces the nonlocal dy-

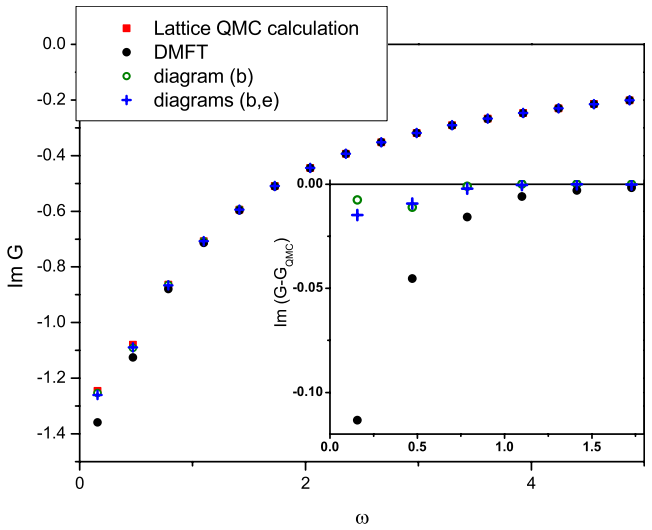

FIG. 8. (Color online) Imaginary part of the local Green's function of undoped Hubbard model at Matsubara frequencies. The data are shown for $U=1, t=0.25, \beta=20$. The reference data are compared with the results of approximate schemes taking antiferromagnetism into account. The results of DMFT calculation, of the scheme with diagram (b), and of the approximation taking two diagrams (b) and (e) into account are shown. Inset shows the deviation of the approximate results from reference data.

namical antiferromagnetic correlations with static ordering, it overestimates the antiferromagnetism in the model. Therefore the pseudogap appears to be too deep; its shoulders and Hubbard bands in the DMFT graph are narrower than they should be. The situation is partly improved for diagram (b): the shoulders and Hubbard bands are closer to the reference curve although the estimation at Fermi energy looks worse. The serious improvement arises from the next diagram of the ladder, as the dashed-dotted curve in Fig. 9 shows. This is

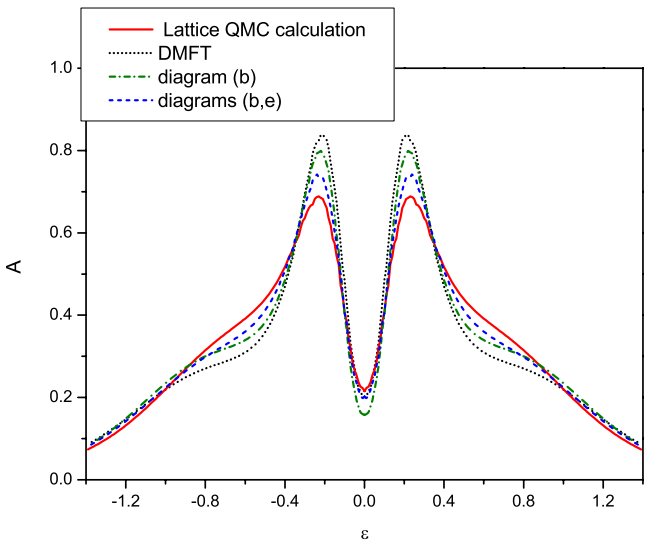

FIG. 9. (Color online) Density of states of the undoped Hubbard model, restored from the data presented in Fig. 8. The approximate result becomes closer to reference data as diagrams (b) and (e) are taken into account.

very expectable because the long-range antiferromagnetic fluctuations are exactly described by these ladders. On the other hand it is interesting to observe from the inset of Fig. 9 that this diagram does not improve the result for $G_{\pi/\beta,r=0}$, but makes its deviation from the reference data more regular.

C. Doped Hubbard: Fermi-arc formation and flattening of the dispersion law

Here we present the results obtained with the dual fermion technique for the pseudogap regime, which corresponds to the doping below optimal and relatively high temperature. We use the rotationally invariant approximation, so the effects of superconductivity and antiferromagnetism were not included in the theory. However it turns out that the theory still captures the physics responsible for the Fermi-arc formation, and yields results which compare well to experimental data.

To make the simulation more realistic we introduce the next-neighbor hopping term t'. The parameters of the model are $U=4.0, t=0.25, t'=-0.075, \beta=80$. The ratio $t'/t \approx -0.3$ roughly corresponds to the case of $YBa_2Cu_3O_7$.[38] The relatively large value of $U=2W$ was taken because there is experimental evidence that the system should be a Mott insulator at small doping, which requires $U>1.5W\approx 3.0$. The temperature used roughly corresponds to 100–150 K, which is a proper value for the pseudogap phenomena in high-temperature superconducting materials. Most of the results are presented on doping level of 14%.

Figure 10 presents the results obtained for the self-energy $\Sigma_{\omega,k}$ at the nodal and antinodal points of the Fermi surface. The position of Fermi surface was defined as a maximum of the spectral density. A polynomial extrapolation for Σ_ω was constructed to obtain the imaginary part of self-energy at Fermi level. One can observe a remarkable difference in the low-energy limit of $\Sigma_{\omega,k}$ at the nodal and antinodal points: the corresponding values of $\mathrm{Im}\Sigma_{\omega=0,k}$ differ approximately by a factor of 2. The spectral function $A_k=(2\pi)^{-1}\mathrm{Im}\, G_{\omega=0,k}$ for the entire Brillouin zone is mapped in Fig. 11 for 14% doping. The Fermi surface in the antinodal direction is quite diffuse, in accordance with the experimental results.

It is worthy to consider the spatial dispersion of the self-energy function. The map of $\mathrm{Im}\,\Sigma_{\omega=0,k}$ is presented in Fig. 12, whereas Fig. 13 shows the behavior of this quantity along the (π,π)-$(\pi,0)$-$(0,0)$-(π,π) contour. The data are obtained with a polynomial extrapolation from Matsubara axis. The estimated error bar of the extrapolation procedure is 0.01. An interesting property of the data obtained is that $\Sigma_{\omega=0,k}$ appears to be substantially nonlocal, but is still short ranged. Actually, the data of Figs. 12 and 13 can be approximately described by the next-neighbor approximation. That is, the most important components of $\Sigma_{\omega=0,R}$ are $\Sigma_{R=(0,0)}$, $\Sigma_{R=(0,1)}$, and $\Sigma_{R=(1,1)}$. The dotted line in Fig. 13 is produced with these Fourier components only, and it is quite consistent with the initial curve except at the points $(\pi,0)$ and $(0,\pi)$, where the self-energy is flattened. It is worthy to notice also that $\mathrm{Im}\,\Sigma_{\omega=0,k}$ is maximal there. Interestingly, variational cluster calculations[39] demonstrate that near the nodal point, in contrast with the antinodal one, the superconducting gap

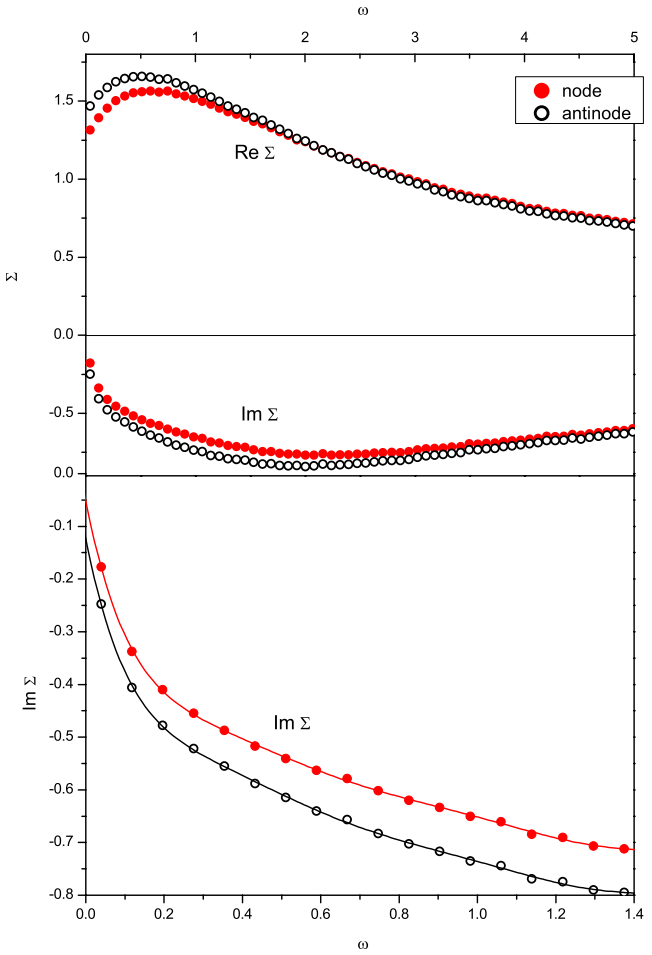

FIG. 10. (Color online) Self-energy function of tt' Hubbard model $\Sigma_{\omega,k}$ at nodal and antinodal points of the Fermi surface at Matsubara frequencies. Diagram (b) is used for the calculations. The data are plotted for 14% doping tt' Hubbard model at $t=0.25, t'=-0.075, U=4.0, \beta=80$. Upper panel: real and imaginary parts of $\Sigma_{\omega,k}$. Lower panel: Im $\Sigma_{\omega,k}$ in a low-frequency region and its approximation with a seventh-order polynomial.

(that is, anomalous part of the self-energy) also can be described in the nearest-neighbor approximation.

Figure 14 shows the effective quasiparticle energy, defined by the formula

$$\epsilon_k^{\text{eff}} = \text{Re}\left[\frac{\epsilon_k - \mu + \Sigma_{\omega=0,k}}{1 + i\dfrac{\partial}{\partial\omega}\Sigma_{k,\omega=0}}\right]. \tag{25}$$

The initial dispersion law ϵ_k is shown in the same figure with thin line. One can see a narrowing of the quasiparticle band, mainly due to the $\partial\Sigma_{\omega,k}/\partial\omega$ term. The latter is large due to closeness to the Mott transition point. Another important change is again the flattening of the curve near $(0,\pi)$ point.

A flattening of the dispersion curve near the antinodal point was earlier predicted[7,9] as due to a non-Fermi-liquid behavior when the Fermi energy crosses Van Hove singularity. The main conclusion of Refs. 7 and 9 is that in the strong-interaction regime Van Hove point expands to a finite

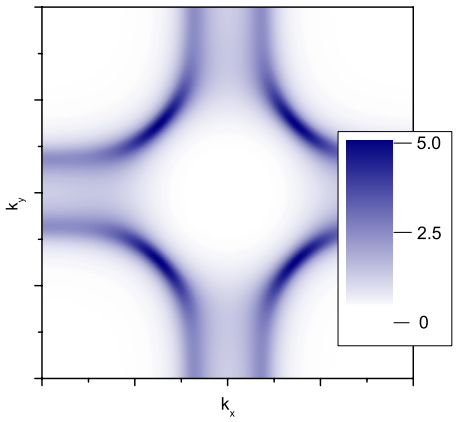

FIG. 11. (Color online) Spectral function $A_{\omega=0,k}$ at Fermi level: the calculation with diagram (b) and polynomial extrapolation from Matsubara frequencies. Parameters of the Hubbard model are the same as in Fig. 10.

region of the Fermi surface, where the dispersion law is flattened. The k dependence of the self-energy and vertex function is of crucial importance for this phenomenon. It is worthy to note that cluster calculation hardly can reproduce the result for the Van Hove behavior because the flattened region is much smaller that the entire Brillouin zone.

We also performed calculations for other dopings. Figure 15 is devoted to Im Σ at 7% doping. Smaller doping makes the system closer to Mott insulator. Therefore the value of Im Σ is substantially larger than for the 14% doped system (Figs. 10 and 13). The flattened regions disappear in this case. However, there is still a clear difference between the nodal and antinodal directions in the low-energy limit: the values of Im $\Sigma_{\omega=0}$ at these points differ by a factor of 2.

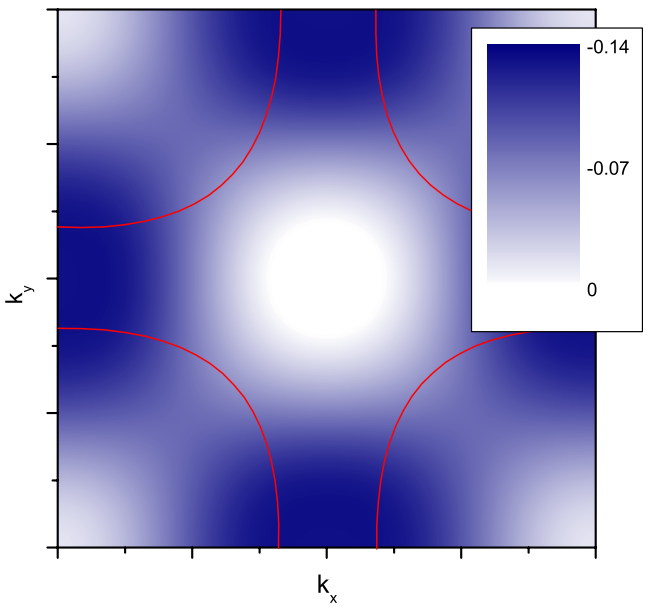

FIG. 12. (Color online) Imaginary part of the self-energy Im $\Sigma_{\omega=0,k}$ at Fermi level: the calculation with diagram (b) and polynomial extrapolation from Matsubara frequencies. Parameters of the Hubbard model are the same as in Fig. 10. The red line indicates Fermi surface.

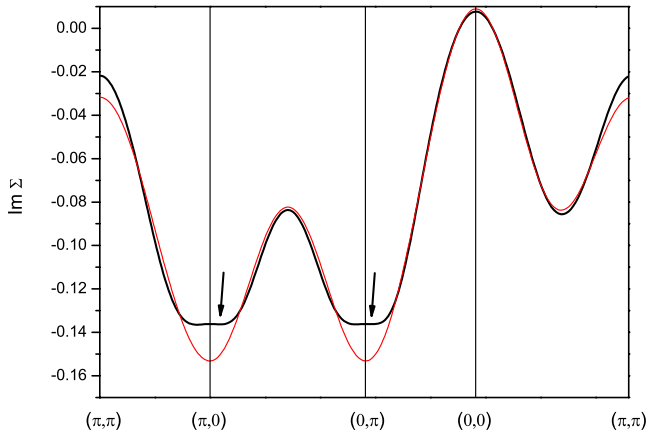

FIG. 13. (Color online) Imaginary part of the self-energy Im $\Sigma_{\omega=0,k}$ at Fermi level: the calculation with diagram (b) and polynomial extrapolation from Matsubara frequencies. Solid line shows the same data as those presented in Fig. 12. Dotted line is a fit with the next-neighbor Fourier components. Arrows mark the flattened region at the antinodal direction. Positive sign of Im $\Sigma_{\omega=0,k}$ in a small region near the (0,0) is probably an artifact of the polynomial extrapolation procedure.

Finally, a few words should be said about the region near (0,0) point in Fig. 13, where our polynomial fit predicted slightly positive Im Σ (that corresponds to Im $G<0$). We argue here that this is merely an artifact of the extrapolation procedure. Indeed, as it is discussed in Sec. II E, negative Im G in our theory could only result from a negative residual. However, the graph of Σ at Matsubara frequencies for all k points is qualitatively similar to those shown in the upper panel of Fig. 15. It is obvious these graphs have a negative derivative at Fermi energy, so that the residual $Z=(i-\frac{\partial\Sigma}{\partial\omega})^{-1}$ must be positive.

IV. CONCLUSIONS

To summarize, the transformation to dual fermion variables completely reconstructs perturbation theory, starting with the zeroth-order approximation which is accurate in the limits of both very weak and very strong interactions. As a result, taking into account just a few lower-order diagrams gives quite satisfactory results, without having to resum infinite series of diagrams. Starting with DMFT as the best local approximation, we are able to take into account nonlocal corrections in a regular perturbative way. In contrast with several cluster approaches, the method is exactly translationally invariant and allows us to analyze how different parts of the reciprocal space are distinctly affected by correlation effects.

This approach can be set up either in phases with long-range order (antiferromagnetism, superconductivity) or in phases without long-range order (normal state) by not allowing for symmetry breaking. The present paper mostly deals with the latter case. By doing so, we could focus on physical effects that are not directly related to incipient long-range order. In particular, we showed that the anisotropic destruction of quasiparticles and the Fermi surface (at least as presented in Figs. 10–14) is not due to precursor effects of antiferromagnetism (or superconductivity) as soon as the intermediate- and strong-coupling regimes are entered. Indeed, it is associated with quite short-range physics, as illustrated by the fact that only the short-range components of the self-energy are found to have significant magnitude. This ob-

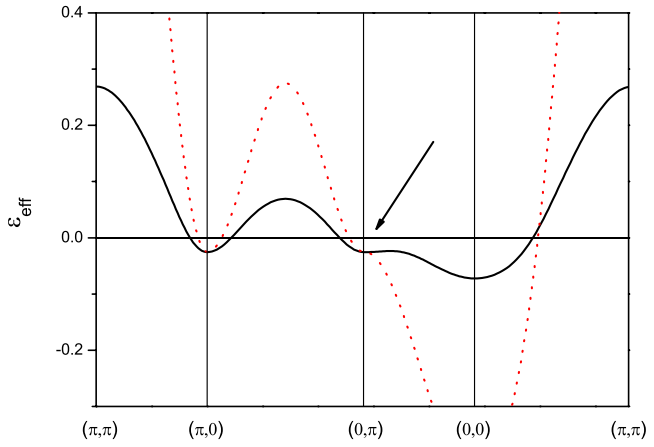

FIG. 14. (Color online) Quasiparticle dispersion law, defined from formula (25) (thick line), compared with initial dispersion (thin line). Model parameters are the same as in Figs. 10–13. Arrows mark the flattening of the Van Hove singularity.

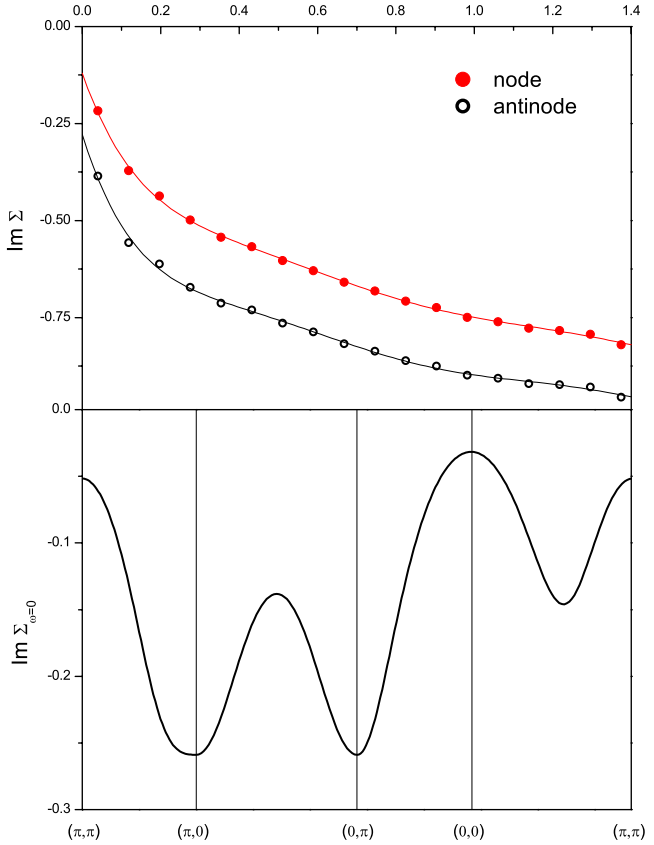

FIG. 15. (Color online) Imaginary part of the self-energy function for the 7% doped system. Other parameters of the tt' Hubbard model are the same as in Figs. 10 and 13. Upper panel: Im Σ at the nodal and antinodal points of the Fermi surface, and its polynomial fit at Matsubara frequencies. Lower panel: low-energy behavior of Im Σ at the (π,π)-$(\pi,0)$-$(0,0)$-(π,π) contour.

servation also provides some support to cluster extensions of DMFT. Although the destruction of quasiparticles in a momentum-selective way is adequately captured by this approach and associated with short-range correlations, more work is required (possibly including symmetry breaking and incipient long-range order) in order to reach a proper description of the pseudogap formation and of its dependence on the doping level and on the t'/t ratio.

ACKNOWLEDGMENTS

The work was supported by RFFI (Grants No. 08-02-01020, No. 08-03-00930, and No. 08-02-91953), DFG (Grant No. 436-RUS-113-938-0), FOM (The Netherlands), CNRS, and Ecole Polytechnique.

APPENDIX A: EXACT RELATIONS FOR HIGH-ORDER CUMULANTS

Similarly to exact relationship (9) between the initial and dual Green's functions, the one-to-one correspondence between higher-order momenta for the initial and dual systems can be established. Particularly, the formula for the fourth-order Green's function was presented and discussed previously.[35] It was shown that the two-particle excitations in the original and dual systems are identical. Here, we use the generating functional approach, which allows us to establish the general structure of such relationships for high momenta, and extend the conclusion about the two-particle excitations to all collective excitations, involving an arbitrary number of particles.

We start from the expression for action (8), which includes both initial and dual variables. Then we introduce the independent variations in initial and dual energies:

$$S[c,c^*,f,f^*;u,v] = S[c,c^*,f,f^*] + u_{12}c_1^*c_2 + v_{12}f_1^*f_2, \tag{A1}$$

where u and v are infinitesimal and a summation over repeating indices is implied.

One can see that Taylor series of the functional

$$F[u,v] = \ln \int e^{-S[c,c^*,f,f^*;u,v]} \mathcal{D}f\mathcal{D}f^*\mathcal{D}c\mathcal{D}c^* \tag{A2}$$

with powers of u and v correspond, respectively, to the cumulants of initial and dual systems. We recall that the second-order cumulant is the Green's function, and higher-order cumulants are proportional to corresponding vertex parts. For example, the fourth-order cumulant is $(\partial^2 F/\partial u_{3'2'}\partial u_{4'1'}) = X_{1234} - G_{23}G_{14} + G_{13}G_{24}$ (X is the two-particle Green's function), whereas the fourth-order vertex is $\Gamma^{(4)}_{1234} = G^{-1}_{11'}G^{-1}_{22'}(\partial^2 F/\partial u_{3'2'}\partial u_{4'1'})G^{-1}_{3'3}G^{-1}_{4'4}$.

To establish a relation between the cumulants, let us integrate over f^*, f in the previous formula. We obtain

$$F[u,v] = F_0[u,v] + \ln \int e^{-S[c,c^*;u,v]} \mathcal{D}c\mathcal{D}c^*,$$

$$F_0[u,v] = -\ln \det \| \mathrm{I} + (\Delta - \epsilon)\alpha^{-1} v \alpha^{-1} \|,$$

$$S[c,c^*;u,v] = S[c,c^*] + \Delta_\omega c^*_{\omega k\sigma} c_{\omega k\sigma} + (u_{12} - M_{12})c_1^* c_2,$$

$$M = [(\Delta - \epsilon)^{-1} + \alpha^{-1} v \alpha^{-1}]^{-1}. \tag{A3}$$

Symbol I in the second line is the matrix unity, and the second term is the product of the corresponding matrices. The fourth line reads similarly.

The last expressions clearly show that the derivatives of $F[u,v]$ with respect to u and v are related. A comparison of the first derivatives, for example, allows one to reproduce formula (9). The last term of Eq. (9) comes from the differentiation of F_0.

Let us consider the fourth-order cumulants $(\partial^2 F/\partial u_{32}\partial u_{41})$ and $(\partial^2 F/\partial v_{32}\partial v_{41})$. First of all we note that neither indices 1 and 2 nor indices 3 and 4 should coincide because otherwise both cumulants vanish due to the Fermi-operator algebra. For the case of different indices, the differentiation is quite simple and gives, after setting $\alpha = g^{-1}$, formula (29) of Ref. 35:

$$\frac{\partial^2 F}{\partial u_{32}\,\partial u_{41}} = L_{11'}L_{22'}\frac{\partial^2 F}{\partial v_{3'2'}\,\partial v_{4'1'}}R_{3'3}R_{4'4}. \tag{A4}$$

Here L and R are matrix inverses of $(\Delta - \epsilon)^{-1}g$ and $g(\Delta - \epsilon)^{-1}$, respectively. It should be emphasized that this expression does not contain any extra additive terms, in contrast to formula (9). Formally this is because the second derivative $(\partial^2 F_0/\partial v_{32}\partial v_{41})$ vanish, as one can check straightforwardly. Physically this means that the two-particle excitations in the original and dual systems are identical.[35]

It might be also instructive to re-express the last formula in terms of vertex function. Setting also $\alpha = g^{-1}$, one obtains

$$\Gamma_{1234} = L'_{11'}L'_{22'}\Gamma^{\mathrm{dual}}_{1'2'3'4'}R'_{3'3}R'_{4'4}, \tag{A5}$$

where $L' = (1 + \Sigma_{\mathrm{dual}}g)^{-1}$ and $R' = (1 + g\Sigma_{\mathrm{dual}})^{-1}$. One can see that the obtained formulas are formally valid also for the case of coinciding indices, when both left- and right-hand sides vanish.

An advantage of the presented approach is that the derivation of the formulas for sixth- and higher-order vertex parts appears to be literally the same as for the fourth-order one. All the argumentation about the absence of the coinciding indices and vanishing of the high derivatives of F_0 is valid for that case. Therefore formula (A5) is valid for vertex parts of any order; just a number of indices and multipliers L', R' should be changed. From the physical point of view, we conclude that all collective excitations of the initial and dual ensembles are the same.

APPENDIX B: FUNCTIONAL MINIMIZATION, RELATION TO DMFT, AND SELF-CONSISTENCY CONDITION

It is clear from the present consideration that a proper choice of the hybridization function Δ is crucial. A functional-minimization scheme is suitable to clarify this issue. Let us introduce a trial action $\tilde{S}[f,f^*]$. For clarity, we put the subscript $\tilde{S}$ at the angular brackets in this appendix, to

emphasize that the averaging is over the system with trial action $\tilde{S}$. We consider Feynman's variational functional

$$\langle \tilde{S} \rangle_{\tilde{S}} + \ln \int e^{-\tilde{S}} \mathcal{D}f \mathcal{D}f^* - \langle S \rangle_{\tilde{S}} - \ln \int e^{-S} \mathcal{D}f \mathcal{D}f^* = \max. \tag{B1}$$

A straightforward variation $\tilde{S} \to \tilde{S} + \delta S$ gives an extremum condition

$$\langle (S - \tilde{S}) \delta S \rangle_{\tilde{S}} = \langle (S - \tilde{S}) \rangle_{\tilde{S}} \langle \delta S \rangle_{\tilde{S}}. \tag{B2}$$

For an arbitrary δS, this indeed means that the extremum of Eq. (B1) is delivered by $\tilde{S}=S$, up to an additive constant. In this case Eq. (B1) vanishes. The larger value of Eq. (B1) corresponds to the better approximation.

There is an important point: since dual action depends on Δ, condition (B1) can be used to determine the optimal Δ. The variation with respect to Δ gives

$$\frac{\delta \langle S \rangle_{\tilde{S}}}{\delta \Delta} = 0. \tag{B3}$$

Here we took into account that variations in $\tilde{S}$ and Δ are independent, so the first two terms of Eq. (B1) do not vary with Δ. As for the last term, it is exactly $\ln Z$ and therefore independent of Δ as well.

Now, recalling $S[f,f^*] = -\ln \int e^{-S[c,c^*,f,f^*]}$ and substituting Eq. (8), we obtain after certain transformations that Eq. (B3) corresponds to the condition

$$G_{\omega,r=0} = \langle g^{\mathrm{imp}}[f_i, f_i^*] \rangle_{\tilde{S}},$$

$$g^{\mathrm{imp}}[f_i, f_i^*] = \frac{\int c_{\omega i}^* c_{\omega i} e^{-S_{\mathrm{site}}[c_i c_i^* f_i f_i^*]} \mathcal{D}c_i^* \mathcal{D}c_i}{\int e^{-S_{\mathrm{site}}[c_i c_i^* f_i f_i^*]} \mathcal{D}c_i^* \mathcal{D}c_i}. \tag{B4}$$

Here S_{site} is defined by formula (10) and $G_{r=0} = N^{-1} \Sigma_k G_k$ is local part of the Green's function. While deriving these formulas, it is useful to take into account that $\alpha = g^{-1}$ is just a scaling factor standing at f^*, f, and there is no need to vary this quantity: one can vary with respect to Δ at fixed α and set $\alpha = g^{-1}$ afterward.

Actually, criterion (B4) has a very clear meaning: local part of the Green's function equals the Green's function of the single-site action S_{site}, averaged over the fluctuations of f. Neglecting these fluctuations, one obtains just a DMFT condition for hybridization function; that is, $G_{\omega,r=0} = g_\omega$.

To make the consideration more clear, let us first consider the Gaussian approximation for dual variables, $\tilde{S} = -\mathcal{G}_{\mathrm{dual}}^{-1} f^* f$. Let us show for this Gaussian trial action, the DMFT condition

$$\mathcal{G}_{\omega,r=0} = g_\omega \tag{B5}$$

satisfies Eq. (B4) *exactly* (call this statement T1). The proof is based on the observation that condition (B5) is equivalent to the requirement that the local part of dual Green's function equals zero,

$$\mathcal{G}_{r=0}^{\mathrm{dual}} = 0, \tag{B6}$$

as one can easily check with formulas (14) and (15). Further, since $\tilde{S}$ is Gaussian, formula (B6) means that all local momenta $\langle f_i^* f_i \rangle, \langle f_i^* f_i f_i^* f_i \rangle, \ldots$ equal zero. It means that local fluctuations of f, f^* are virtually absent; therefore $\langle g_\omega^{\mathrm{imp}}[f, f^*] \rangle = g_\omega$ and Eq. (B4) becomes Eq. (B5). To obtain a formal proof, one should consider an average of the Taylor series for $g^{\mathrm{imp}}[f, f^*]$. This series starts from g_ω, whereas the average of any higher term vanishes. This proves T1.

Next, it is possible also to show that the DMFT Green's function is optimal with respect to the variations in the Gaussian trial action (call this statement T2). With a variation $\tilde{S} = -\mathcal{G}_{\mathrm{dual}}^{-1} f^* f \to \tilde{S} = -\mathcal{G}_{\mathrm{dual}}^{-1} f^* f + 0 f_1^* f_2$, formula (B2) becomes

$$\langle (S + \mathcal{G}_{\mathrm{dual}}^{-1} f^* f) f_1^* f_2 \rangle_{\tilde{S}} = \langle S + \mathcal{G}_{\mathrm{dual}}^{-1} f^* f \rangle_{\tilde{S}} \langle f_1^* f_2 \rangle_{\tilde{S}}. \tag{B7}$$

The essential point is again that since all local momenta of f, f^* are vanished because of Eq. (B6) and the dual potential V is local in space, all the nonlinearity drops out from Eq. (B7). It means that both left- and right-hand sides of Eq. (B7) equal the same value if $-\mathcal{G}_{\mathrm{dual}}^{-1} f^* f$ equals the Gaussian part of the dual action. This proves T2. Thus, we have shown that the DMFT procedure can be considered as the Gaussian approximation for the dual variables, which is optimal in the sense of Feynman minimization criterion, with respect to both trial action and hybridization function.

Beyond the Gaussian trial action, an analytical treatment of extremal criterion (B1) is hardly possible. Therefore, in the main body of the theory we treat the dual system perturbatively, using the diagram series with respect to V and the hybridization function defined from condition (19).

[1] A. Georges, G. Kotliar, W. Krauth, and M. J. Rozenberg, Rev. Mod. Phys. **68**, 13 (1996).

[2] T. Moriya, *Spin Fluctuations in Itinerant Electron Magnetism* (Springer, Berlin, 1985).

[3] A. C. Hewson, *The Kondo Problem to Heavy Fermions* (Cambridge University Press, Cambridge, 1993).

[4] T. Giamarchi, *Quantum Physics in One Dimension* (Oxford University Press, Oxford, 2004).

[5] P. W. Anderson, *The Theory of Superconductivity in the High-T_c Cuprates* (Princeton University Press, Princeton, NJ, 1997).

[6] D. J. Scalapino, Phys. Rep. **250**, 329 (1995).

[7] I. E. Dzyaloshinskii, J. Phys. I **6**, 119 (1996).

[8] C. J. Halboth and W. Metzner, Phys. Rev. B **61**, 7364 (2000); Phys. Rev. Lett. **85**, 5162 (2000).

[9] V. Yu. Irkhin, A. A. Katanin, and M. I. Katsnelson, Phys. Rev. B **64**, 165107 (2001); Phys. Rev. Lett. **89**, 076401 (2002).

[10] J. Schafer, M. Hoinkis, Eli Rotenberg, P. Blaha, and R. Claessen, Phys. Rev. B **72**, 155115 (2005).
[11] G. Kotliar, S. Savrasov, K. Haule, V. Oudovenko, O. Par-collet, and C. Marianetti, Rev. Mod. Phys. **78**, 865 (2006).
[12] T. Maier, M. Jarrell, T. Pruschke, and M. H. Hettler, Rev. Mod. Phys. **77**, 1027 (2005).
[13] A. I. Lichtenstein and M. I. Katsnelson, Phys. Rev. B **62**, R9283 (2000).
[14] K. Haule and G. Kotliar, Phys. Rev. B **76**, 104509 (2007).
[15] A. I. Poteryaev, A. I. Lichtenstein, and G. Kotliar, Phys. Rev. Lett. **93**, 086401 (2004).
[16] A. Toschi, A. A. Katanin, and K. Held, Phys. Rev. B **75**, 045118 (2007).
[17] H. Kusunose, J. Phys. Soc. Jpn. **75**, 054713 (2006).
[18] C. Slezak, M. Jarrell, Th. Maier, and J. Deisz, arXiv:cond-mat/0603421 (unpublished).
[19] A. N. Rubtsov, M. I. Katsnelson, and A. I. Lichtenstein, Phys. Rev. B **77**, 033101 (2008).
[20] A. N. Rubtsov, Phys. Rev. B **66**, 052107 (2002).
[21] S. Sarker, J. Phys. C **21**, L667 (1988).
[22] D. Boies, C. Bourbonnais, and A.-M. S. Tremblay, Phys. Rev. Lett. **74**, 968 (1995).
[23] T. D. Stanescu and G. Kotliar, Phys. Rev. B **70**, 205112 (2004).
[24] A. Georges and J. S. Yedidia, J. Phys. A **24**, 2173 (1991).
[25] G. Baym and L. P. Kadanoff, Phys. Rev. **124**, 287 (1961); G. Baym, *ibid.* **127**, 1391 (1962).
[26] C. Itzykson and J.-B. Zuber, *Quantum Field Theory* (McGraw-Hill, New York, 1980).
[27] A. N. Rubtsov, arXiv:cond-mat/0302228 (unpublished); A. N. Rubtsov and A. I. Lichtenstein, JETP Lett. **80**, 61 (2004); A. N. Rubtsov, V. V. Savkin, and A. I. Lichtenstein, Phys. Rev. B **72**, 035122 (2005).
[28] Th. Maier, M. Jarrell, Th. Pruschke, and J. Keller, Phys. Rev. Lett. **85**, 1524 (2000).
[29] C. Huscroft, M. Jarrell, Th. Maier, S. Moukouri, and A. N. Tahvildarzadeh, Phys. Rev. Lett. **86**, 139 (2001).
[30] A. Macridin, M. Jarrell, T. Maier, P. R. C. Kent, and E. D'Azevedo, Phys. Rev. Lett. **97**, 036401 (2006).
[31] T. A. Maier, M. Jarrell, and D. J. Scalapino, Phys. Rev. B **74**, 094513 (2006).
[32] A. Macridin and M. Jarrell, Phys. Rev. B **78**, 241101(R) (2008).
[33] D. R. Hamann and S. B. Fahy, Phys. Rev. B **41**, 11352 (1990).
[34] A. Kampf and J. R. Schrieffer, Phys. Rev. B **41**, 6399 (1990).
[35] S. Brener, H. Hafermann, A. N. Rubtsov, M. I. Katsnelson, and A. I. Lichtenstein, Phys. Rev. B **77**, 195105 (2008).
[36] H. Hafermann, S. Brener, A. N. Rubtsov, M. I. Katsnelson, and A. I. Lichtenstein, Pis'ma Zh. Eksp. Teor. Fiz. **86**, 769 (2007).
[37] R. Chitra and G. Kotliar, Phys. Rev. Lett. **83**, 2386 (1999).
[38] O. K. Andersen, A. I. Liechtenstein, O. Jepsen, and F. Paulsen, J. Phys. Chem. Solids **56**, 1573 (1995).
[39] M. Aichhorn, E. Arrigoni, Z. B. Huang, and W. Hanke, Phys. Rev. Lett. **99**, 257002 (2007).